Journal of The Electrochemical Society, **153** (4) C235-C241 (2006)
0013-4651/2006/153(4)/C235/7/$20.00 © The Electrochemical Society

An In Situ Ellipsometric Study of Cl^--Induced Adsorption of PEG on Ru and on Underpotential Deposited Cu on Ru

Marlon L. Walker,[a,z] Lee J. Richter,[a] Daniel Josell,[b] and Thomas P. Moffat[b,*]

[a]*Chemical Sciences and Technology Laboratory, and* [b]*Material Science and Engineering Laboratory, National Institute of Standards and Technology, Gaithersburg, Maryland 20899, USA*

The adsorption of polyethylene glycol and chloride ion (PEG–Cl^-) on (*i*) air-oxidized Ru (native oxide), (*ii*) "activated" Ru (electrolytic reduction of the native oxide), and (*iii*) underpotential deposited (UPD) Cu on activated Ru was examined in situ using spectroscopic ellipsometry. In the absence of Cl^-, PEG adsorption was minimal at all relevant potentials on the activated Ru and Cu UPD surfaces characterized in this study. On activated Ru, the addition of Cl^- ion resulted in enhanced PEG coadsorption. At potentials relevant to Cu UPD, a three-component PEG–Cl^-–Cu layer formed independent of the order of additive addition to the electrolyte. The PEG–Cl^-–Cu UPD overlayer provided inhibition of subsequent Cu overpotential deposition. At potentials positive of Cu UPD, a monolayer oxide film formed on Ru that inhibited PEG adsorption even in the presence of Cl^-. Slight PEG adsorption was observed on Ru native oxide surfaces, although there was no enhancement observed in the presence of Cl^-. Ru oxidation exerted a strong effect on the adsorption of additives that was directly relevant to the nucleation and growth of electrodeposited Cu.
 [DOI: 10.1149/1.2170587]

Manuscript submitted August 30, 2005; revised manuscript received December 13, 2005.
Available electronically February 24, 2006.

Over the last eight years Cu has become the material of choice for on-chip interconnect metallization of electronic devices.[1] Superconformal Cu electrodeposition is key to the void-free filling of trenches and vias for these interconnects. The bottom-up superconformal growth dynamic ("superfilling") is achieved by using electrolytic plating baths containing additives such as chloride ion (Cl^-), polyethylene glycol (PEG), and sulfonate-terminated disulfides such as $Na_2[SO_3(CH_2)_3S]_2$ (SPS) that inhibit (PEG–Cl^-) and accelerate (SPS–Cl^-), respectively, the rates of electrodeposition.[2] Superfilling of trenches and vias by Cu electrodeposition arises from a competition for surface sites between the rate-accelerating SPS vs deposition-inhibiting PEG. In a conventional electrolyte the PEG-based inhibiting layer forms rapidly upon immersion of a Cu substrate while, subsequently, the more strongly binding SPS displaces PEG from the surface. The effect is accentuated on concave geometries, such as the bottoms of trenches and vias, where area reduction during growth results in lateral SPS–PEG interaction that leads to the expulsion of the latter and accelerated bottom-up copper superfilling.[2]

As the width of on-chip interconnect wiring shrinks below the 70-nm length scale, attention is being focused on strategies that minimize increases in the resistance of the conductors. Present interconnect architectures involve the use of Ta, TaN, or related barrier materials to isolate the Cu wiring from the surrounding dielectric.[3] The barrier materials are deposited onto the patterned dielectrics on Si wafer substrates using variants of physical vapor deposition (PVD) or chemical vapor deposition (CVD). Attempts have been made to directly electrodeposit Cu on TaN and TiN barriers, but difficulties were encountered in obtaining smooth, flat coalesced layers due to Cu wetting issues.[4,5] Additionally, films produced by direct electrodeposition on TaN and TiN were often characterized by poor adherence to the substrate.[5,6] As a consequence, a Cu seed layer is deposited on the barrier layer by PVD/CVD or electroless deposition (for example, Ref. 7) prior to electrodeposition. The Cu seed acts as a wetting layer for the subsequent Cu superfilling electroplating process. The Cu seed also provides an enhanced conductive path between the wafer edge contact and other points on the wafer that helps minimize the nonuniform deposition potential, i.e., terminal effect, associated with resistive barrier materials.[8-10] Extension of the above methodology to deep sub-100-nm interconnects presents a significant challenge because the seed layer/barrier layer combination represents an increasing fraction of the cross-sectional area of the metallization.

Recently, Ru[11-13] was among several metals (including Pt, Ag, Pd, Ir and Rh)[13] proposed as new barrier materials for the Cu damascene process. Ru has negligible solubility with Cu and an electrical resistivity (7.6 $\mu\Omega$ cm) that is half that of current barrier materials such as Ta. The interdiffusion characteristics of electroplated Cu on sputtered polycrystalline 20-nm Ru films on Si were found to be minimal below 450°C.[14] More recently, Rutherford back-scattering (RBS) studies of interdiffusion between Cu and a 5-nm-thick Ru barrier revealed that the Cu/Ru interface was stable during annealing at temperatures up to 300°C.[15] Excellent adhesion was observed between electroplated Cu and Ru.[14] The prospective barriers also offer the possibility, and associated technical and economic advantages, of direct Cu electrodeposition without the need for a Cu seed layer, i.e., "seedless superfill." Several reports of direct superconformal Cu deposition in trenches and vias with Ru barrier layers have been reported.[7,12] More recently, in a companion study to this work, the nature of feature filling was shown to be a sharp function of the surface state of Ru.[16] In particular, the extent of Ru oxidation was shown to have a major effect on the nucleation and growth of electrodeposited Cu. Effective feature filling was observed only on barriers that had minimal exposure to the atmosphere or were pretreated to reduce the air-formed native oxide. Successful feature superfilling and control of its sensitivity to the surface state of Ru requires an understanding of the adsorption of plating additives on both Ru and Cu as well as the effect of oxidation and other pretreatments. A particularly interesting aspect of the proposed barrier materials, e.g., Ru, Pt, etc., is the well-known propensity for Cu underpotential deposition (UPD) on the respective clean metal surface.[16-23] The Cu UPD layer, which can be formed prior to bulk copper deposition, may act as a "seed" or wetting layer that aids superfilling of fine features. The UPD process also provides a convenient electrochemical probe of the surface state of the as-deposited barrier metals.[23]

Central to effective Cu superfilling is the rapid formation of a PEG–Cl^- inhibiting film upon initial immersion into the plating bath. Several studies have demonstrated the inhibiting character of PEG on Cu deposition and a variety of proposals as to the nature and manner of its operation have been put forth.[24-37] In order to investigate these questions in more detail, in situ spectroscopic ellipsometry has been used to characterize PEG/Cl^- coadsorption on the coinage metals Cu, Ag, and Au.[31] At potentials positive of the potential-of-zero charge (pzc), adsorption of PEG in a Cl^--free electrolyte is minimal. In contrast, PEG coadsorption in the presence of Cl^- yields a ~0.6-nm-thick organic overlayer. A similar thickness

* Electrochemical Society Active Member.
z E-mail: marlon.walker@nist.gov

organic layer is formed in the presence of Cl^- on Ag and Au surfaces,[31] thereby calling into question a previously proposed mechanism for PEG adsorption on Cu that involved Cu^+ or Cu^{2+}. In this paper we examine PEG–Cl^- adsorption on Ru. Specifically, the adsorption of PEG–Cl on (*i*) air-oxidized Ru (native oxide), (*ii*) "activated" Ru (the native oxide electrolytically reduced), and (*iii*) UPD Cu on activated Ru was examined using in situ spectroscopic ellipsometry and voltammetry.

Experimental

The electrolytic solutions used in this study were prepared from ultrapure 18.2 MΩ water that was UV-irradiated to remove trace organics (Barnstead Nanopure Diamond).[c] The base electrolyte, 1.8 mol/L H_2SO_4 (made from 98% H_2SO_4, Sigma), was used to make solutions of the appropriate concentration of PEG (3400 g/mol M.W. Aldrich), NaCl (Aldrich), and $CuSO_4 \cdot 5H_2O$ (Aldrich) such that when aliquots were added to the in situ cell, the concentrations of additives in the cell were 88 μmol/L, 1 mmol/L, and 10 m mol/L, respectfully. Thin film polycrystalline Ru working electrodes were prepared by electron-beam evaporation onto Si(100) wafers that were primed with a 2-nm Ti adhesion layer. Two thicknesses of Ru were examined; 6.5 and 100 nm. The latter proved to be quite rough[16] and were thus used only for preliminary experiments. All the data presented in this paper was collected using 6.5-nm-thick Ru films. Background electroanalytical experiments probing Ru oxide formation, reduction and Cu UPD were performed in a conventional deaerated, three-electrode electrochemical cell at 50 mV/s sweep rate. For optical measurements Ru substrates were secured in a custom-built Teflon electrochemical cell designed for in situ spectroscopic ellipsometric measurements; a more complete description of the cell and its use can be found elsewhere.[31] A saturated $K_2SO_4/Hg_2SO_4/Hg$ [mercurous sulfate electrode (MSE)] reference electrode was used in halide-sensitive experiments while a saturated calomel reference electrode (SCE) was deemed suitable for experiments initially including Cl^-. A Pt wire counter electrode was situated in the cell opposite the working electrode, while the reference electrode was located just above the working electrode. In this paper all potentials are reported with respect to SCE.

A Woollam M2000D spectroscopic ellipsometer was used to probe interactions at the electrode–electrolyte interface. The spectrometer measures the ellipsometric angles Ψ and Δ for 508 wavelengths from 193 to 1000 nm simultaneously, allowing the study of time-dependent phenomena. The parameters Ψ and Δ are related to the complex Fresnel parallel and perpendicular polarization reflection coefficients r_p and r_s by the relation

$$\tan \Psi \exp(i\Delta) = \frac{r_p}{r_s}$$

Model calculations for both dynamic and spectroscopic modes of the instrument were performed using the vendor-supplied software package.

Optical experiments began by filling the cell with electrolyte, followed by immediate application of the desired potential. The optical constants of the immersed Ru substrate evolved with time and were allowed to stabilize before commencing additive addition. PEG and Cl^- were introduced to the cell by mixing an aliquot (~100 μL) of concentrated solution in a clean beaker with a significant fraction of electrolyte withdrawn from the contents of the cell. The withdrawn fraction was then reintroduced to the cell with sufficient agitation for adequate mixing. Enough electrolyte remained in the cell during the exchange to maintain potential control. To ensure this process did not perturb the sample, or in any way affect the ellipsometric measurement, the procedure was also done without additive additions as a control to define baseline stability (cycling).

A three-phase planar interface model was used to interpret and parameterize the ellipsometric data. The model consists of a substrate phase characterized by a complex dielectric function ε_s, a model film with thickness t, and dielectric function ε_f, and the ambient electrolyte characterized by dielectric function ε_e. The effective dielectric function and the thickness of the film reflect the polarizability of the metal surface, and thus, the net surface charge and potential, as well as the orientation and identity of species in the inner Helmholtz layer and aspects of the outer Helmholtz layer.[33-35] Changes to the metal potential generally change the net surface charge, resulting in a change in optical response even in the absence of changes in adsorbed species. Therefore all quantitative measurements of adsorption were done at constant potential.

The ambient electrolyte was modeled by a Cauchy function of the form $\varepsilon_e(\lambda) = (n_0 + b/\lambda^2)^2$ with $n_0 = 1.3439$ and $b = 0.003095$ nm^2. The substrate dielectric function ε_s was derived for each sample substrate by direct inversion of the spectroscopic ellipsometric data recorded at 0.050 V_{SCE} (i.e., after reduction of the native oxide). The film, expected to be PEG in the additive experiments, was modeled with a dielectric constant of bulk PEG, 1.455.[d] The effective dielectric constant for a monolayer of Cl^- is anticipated to reflect both the polarizability of the Cl^- and charge rearrangement in the metal. We have used the same dielectric function used for the film, ε_f, to model the adsorbed Cl^-. The Cl^- model thickness is thus not to be interpreted as physical; the use of ε_f is descriptive and adequate for the purpose of tracking coadsorption processes. Similarly, the same dielectric function ε_f was also used in interpreting the Cu UPD and overpotential deposition (OPD) layers; again, the Cu model thickness should not be interpreted as an accurate physical thickness.

Results

Electroanalytical Experiments.— Oxide formation on Ru and its reduction.— As-received PVD Ru is covered with an air-formed oxide film. Immersion into 1.8 mol/L H_2SO_4 + 1 mmol/L NaCl that is open to the laboratory ambient yields an open circuit potential ranging from 0.62 to 0.76 V_{SCE}. The air-formed oxide film can be removed by polarization at negative potentials, typically in or approaching the hydrogen evolution region. An effective activation treatment involves stepping the potential to −0.2 V_{SCE} for 30 s.[16] Voltammetry shown in Fig. 1 reveals a reduction wave centered near −0.150 V_{SCE} that is ascribed to reduction of the three-dimensional air-formed oxide film, corresponding to a charge of ~3 mC/cm^2; ellipsometry reveals a corresponding optical signature that is detailed later. In this paper electrodes treated in this manner are referred to as "activated."

The effect of subsequent oxidation of activated Ru at more positive potentials is readily examined by voltammetry. For oxidation below 0.5 V_{SCE} a broad reduction peak centered near 0.175 V_{SCE} is apparent as shown in Fig. 1. Integrating between 0.5 and −0.150 V_{SCE} yields a reduction charge of ~0.45 mC/cm^2. Prior work with polished polycrystalline, as well as single-crystal Ru electrodes, indicates that oxidation in this potential regime is a one-electron process, $Ru + H_2O \rightarrow RuOH + H^+ + e^-$, that is nominally chemically reversible and constrained to the monolayer level ~0.26 mC/cm^2.[21,36,37] The larger charge observed here can be attributed to a combination of increased surface area and defect density of the polycrystalline PVD films.[21,38-40] Using the charge of monolayer oxidation for area calibration, the electroactive area of the 6.5-nm-thick Ru, is determined to be 1.7 times greater than its nominal area.

[c]Certain commercial equipment, instruments, or materials are identified in this paper to foster understanding. Such identification does not imply recommendation or endorsement by the National Institute of Standards and Technology, nor does it imply that the materials or equipment identified are necessarily the best available for this purpose.

[d]The index of refraction value used is from a publication of the Clariant Company for a product similar in molecular weight and texture as the one used in these experiments.

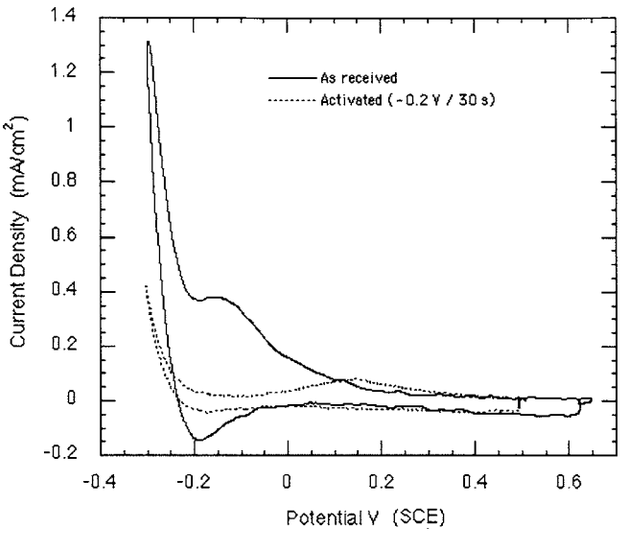

Figure 1. Voltammetry showing reduction of the air-formed oxide on as-received Ru (solid) and the reversible formation and reduction of the monolayer oxide formed on activated Ru (dashed). Cathodic currents are positive.

Cu UPD.— Once the 3D air-formed oxide has been removed, Cu UPD is readily observed on the Ru when $CuSO_4$ is added to the H_2SO_4/Cl^- electrolyte. As shown in Fig. 2 the deposition wave is centered near 0.05 V_{SCE}. The process is kinetically hindered, as evident from the 0.065-V peak separation between the deposition and stripping waves. Reduction of the monolayer oxide species also occurs in this regime, as shown by the background voltammogram in Fig. 2. It is possible that the oxide reduction process controls the onset of the Cu UPD reaction.[21] Integration of the UPD wave between 0.5 and 0.0 V_{SCE}, followed by subtraction of the background current associated with monolayer oxide reduction, yields a charge of 1 mC/cm^2. Prior work using mechanically polished Ru[21] in H_2SO_4/Cl^- ascribes a charge of ~0.6 mC/cm^2 to a close-packed monolayer of Cu(111)/Ru(0001). Other experiments in perchloric acid also found 0.6 mC/cm^2.[20,22] The similar work functions of Cu and Ru in combination with radiotracer studies[41] suggest that while

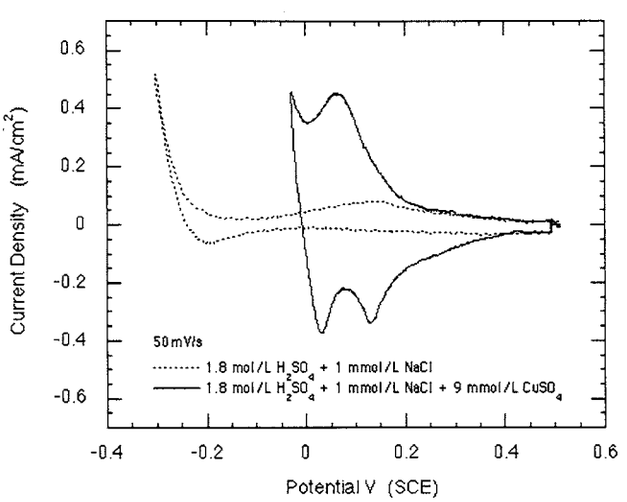

Figure 2. Voltammetry of an activated Ru electrode showing Cu UPD at ~0.05 V followed by bulk Cu deposition and subsequent stripping of the respective Cu layers (solid). Background voltammetry showing that the onset of reduction of the monolayer oxide is coincident with Cu UPD (dashed). Cathodic currents are positive.

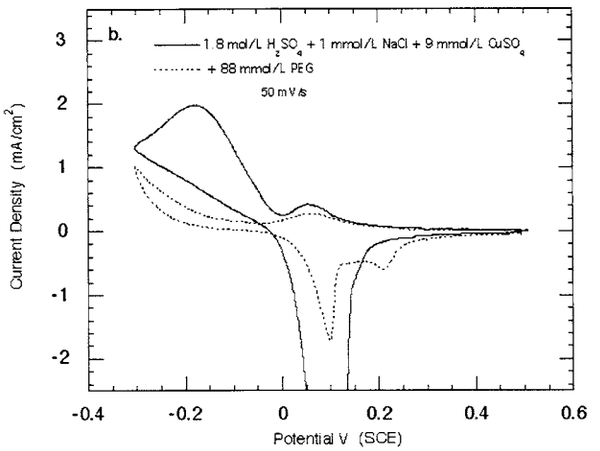

Figure 3. Voltammetry probing the effect of PEG addition on Cu(UPD) and Cu(OPD) on Ru. Cathodic currents are positive.

Cl^- adsorption occurs in this system, the difference in coverage on Ru vs Cu yields only a small fraction of the total charge exchanged during Cu UPD on Ru. The full 1 mC/cm^2 charge is therefore taken to be Cu UPD. Assuming the 0.6 mC/cm^2 monolayer Cu UPD charge, a roughness factor of 1.7 is obtained for the 6.5-nm Ru film, consistent with the value derived from oxide reduction.

If the voltammetric scan range is extended as in Fig. 3, bulk Cu electrodeposition occurs below 0.00 V_{SCE}, the reaction becoming diffusion-limited beyond −0.2 V_{SCE}. Both bulk deposition and formation of the Cu UPD layer are chemically reversible, as reflected in the respective stripping waves shown in Fig. 2 and Fig. 3.

When PEG is added to the electrolyte the charge associated with the Cu UPD process is somewhat diminished but the peak potential is unperturbed; the constant peak potential is consistent with the kinetics of the Cu UPD being controlled by monolayer oxide reduction, as suggested earlier. In contrast, while the peak current of the UPD desorption wave is also only slightly attenuated by PEG coadsorption, there is a 50-mV shift of the peak to more positive potential, suggesting stabilization of the UPD Cu is provided by coadsorbed PEG–Cl^-.[16] This is consistent with the inhibition of anodic dissolution of bulk Cu films by PEG–Cl^-.[42] Importantly, when the potential is swept to more negative values, the PEG interacts with the Cu UPD layer to provide significant inhibition of Cu OPD, as is evident in Fig. 3.

Spectroscopic ellipsometry.— PEG–Cl^- adsorption and Cu UPD on activated Ru.— As indicated in Fig. 1 the native oxide layer may be reduced (Ru activation) by stepping the potential to values negative of −0.2 V_{SCE}. Attention is focused on the adsorption of PEG–Cl^- at 0.05 V_{SCE}, a value corresponding to the peak for Cu UPD, as shown in Fig. 2 and 3. Two conditions of the Ru surface are examined: the activated state and the same with the addition of a Cu UPD layer. Ellipsometry data is summarized by tracking the model thickness of the adsorbed surface film as the potential or solution composition is varied.

In Fig. 4a, an as-received Ru specimen is initially biased at 0.50 V_{SCE}. Upon stepping the potential to −0.30 V_{SCE}, a substantial reduction in the model thickness is evident. This change convolves the reduction of the native oxide, the change in the metal polarizability due to the change in potential, and the development of a hydrogen layer (as −0.30 V_{SCE} is below the potential for hydrogen reduction).[16] After approximately 1 min, the potential was stepped back to 0.500 V_{SCE}, with only a minor change in model thickness as compared to that accompanying the reduction step. This small change convolves the desorption of the hydrogen layer and adsorption of the monolayer oxide (Fig. 1) along with any change in the metal polarizability. The sample was allowed to stabilize at

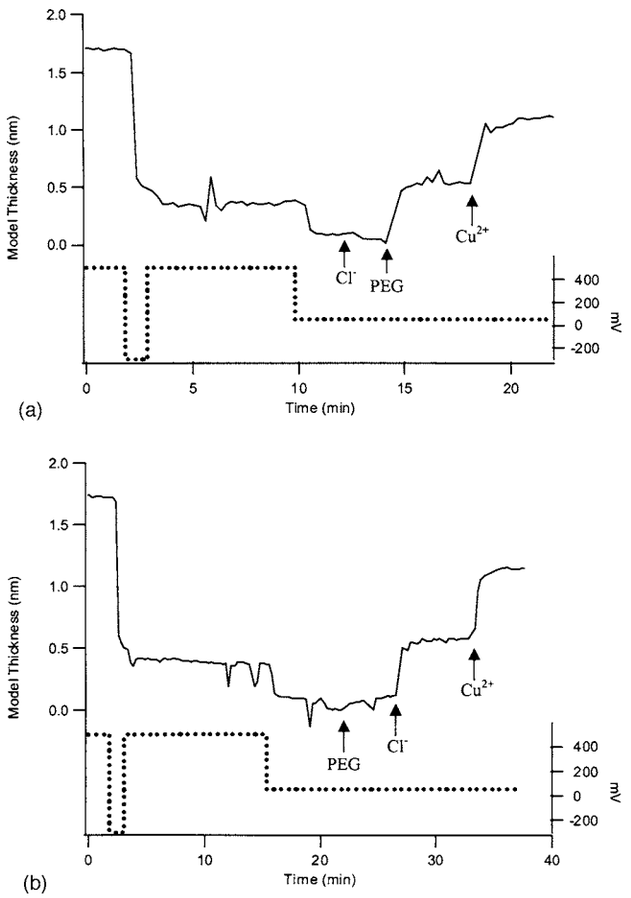

Figure 4. (a) Model thickness (solid line) of an experimental run on an activated Ru surface in which Cl^- was added first (12 min), followed by PEG (14 min) and Cu^{2+} (18 min), with all additions made at 0.050 V. (b). Model thickness (solid line) of an experimental run on an activated Ru surface in which PEG was added first (24 min), followed by Cl^- (26 min) and Cu^{2+} (32 min), with all additions made at 0.050 V. The history of the applied potential is given by the dotted line in each case.

0.50 V_{SCE}. The small peak at ~6 min is due to a controlled cycling, verifying baseline stability. At approximately 10 min, the potential was stepped to 0.050 V_{SCE}, with a drop in the model thickness accompanying reduction of the monolayer oxide that had formed at 0.50 V_{SCE}.

Changes in the model thickness associated with a particular event (i.e., a potential changes or the introduction of an additive) were quantified by averaging the 8–10 data points preceding and following an event; the uncertainty for all stated values is no more than 0.02 nm at one standard deviation. The ratio of the change in the model thickness associated with monolayer oxide reduction to that for the reduction of the original air-formed oxide film is 0.2, close to the 0.15 ratio in charge obtained voltammetrically (i.e., Fig. 1). There was no detectable change in model thickness at 12 min when Cl^- was added. At 14 min, PEG was introduced, with a concurrent increase in the interface thickness to 0.49 nm. Cu was added at 18 min, inducing a further 0.57-nm increase of the model thickness due to Cu UPD.

In Fig. 4b the experiment was repeated but with the order of the PEG and Cl^- additions reversed. After the reduction of the native oxide during the first 2 min, the sample was biased at 0.50 V_{SCE} and baseline stability established. The potential was then stepped to 0.050 V_{SCE}, where the oxide formed at 0.50 V_{SCE} was reduced. The PEG was added first at 23.6 min. There was a small change of 0.03 nm, indicating minimal adsorption of PEG on the electrode. Upon addition of Cl^-, the model thickness increased to 0.47 nm, statistically identical to the value found for the reverse order of additions. Upon addition of Cu, the model thickness increased by 0.56 nm due to Cu UPD, the value again statistically identical to the earlier finding.

The above experiments demonstrate that significant PEG adsorption on Ru only occurs when PEG and Cl^- are both present in the electrolyte. This is congruent with previous results for PEG–Cl^- adsorption on the coinage metals Au, Ag, and Cu, using spectroscopic ellipsometry,[31] Raman,[24] and electrochemical quartz crystal microbalance (EQCM) techniques[28] and consistent with arguments based on the pzc for anion adsorption. Interestingly, chloride adsorption is known to occur on Ru[37,41] in this potential regime but is not directly detectable in our experiment. However, the presence of absorbed Cl^- can be inferred from the subsequent PEG adsorption behavior. The failure to observe a Cl^- layer on Ru with spectroscopic ellipsometry suggests that there is a fortuitous cancellation between the dielectric contribution of the adsorbed ion (and displacement of any sulfate/ bisulfate[21]) and the charge-transfer-induced change in the metal polarizability. The Cu UPD occurs readily on the PEG–Cl^- covered Ru surface, and its formation is not effected by the order of PEG–Cl^- addition.

The same experiment was repeated but with a Cu UPD layer being formed first, followed by Cl^- and PEG additions. The previously observed behavior during the reduction and hold cycle is visible at early times in Fig. 5a. Beginning at around 26 min, the potential was alternated between 0.500 and 0.050 V_{SCE} to assure sample baseline stability with thickness changes corresponding to reduction (at 0.05 V_{SCE}) and formation (at 0.50 V_{SCE}) of the monolayer oxide and associated changes in the metal polarization. At 38 min the potential was stepped to 0.050 V_{SCE} and held. Cu was added at 43 min and the model thickness changed by 0.50 nm. This is similar to the model thickness change seen in Fig. 4 and is consistent with the observed minimal differences between Cu UPD on polycrystalline surfaces in either the presence or absence of Cl^- (see Ref. 21). At 49 min Cl^- was added, inducing a 0.19-nm increase in model thickness. The addition of PEG at 54 min resulted in an additional increase of 0.61 nm.

In Fig. 5b the order of PEG and Cl^- addition was reversed from that in Fig. 5a. After the establishment of a stable baseline, Cu was added at 27 min, with a model thickness increase of 0.52 nm. The addition of PEG at 33 min was accompanied by virtually no detectable change, similar to the behavior observed in the absence of UPD Cu (Fig. 4b). When Cl^- was added at 37 min, the model thickness increased by 0.9 nm.

The observations with regard to PEG–Cl^- and Cl^-–PEG adsorption on the Cu UPD layer are almost indistinguishable from those noted above for the adsorption directly on the Ru. On neither surface was there significant adsorption of PEG in the absence of Cl^-. However, unlike on Ru, the adsorption of Cl^- on the Cu UPD layer results in an ellipsometrically detectable model film thickness change. The ~0.18 nm thickness found for this layer is a factor of 3 smaller than the 0.57 ± 0.17 nm value reported in earlier studies of Cl^- on bulk Cu at more negative potentials.[31]The dependence of the optical characteristics of the Cl^- monolayer on substrate characteristics, i.e., being nearly undetectable on Ru while having strong contrast on the coinage metals [31] and intermediate contrast on a Cu UPD layer, supports the assertion that the optical response of the adsorbed Cl^- arises from a competition between substrate polarization and adsorbate dielectric contributions. This is consistent with the observation that the effective optical constants of the Cl^- layer formed on bulk Cu had some substrate character.[31]

The thicknesses for PEG–Cl^- adlayers on Ru and the Cu UPD layer on Ru summarized in Table I do show run-to-run variability as indicated by the standard deviations. Nonetheless, the thickness of the PEG layer on both surfaces (δPEG) as determined from the difference of the combined Cl^-–PEG value and the Cl^- value (0.42

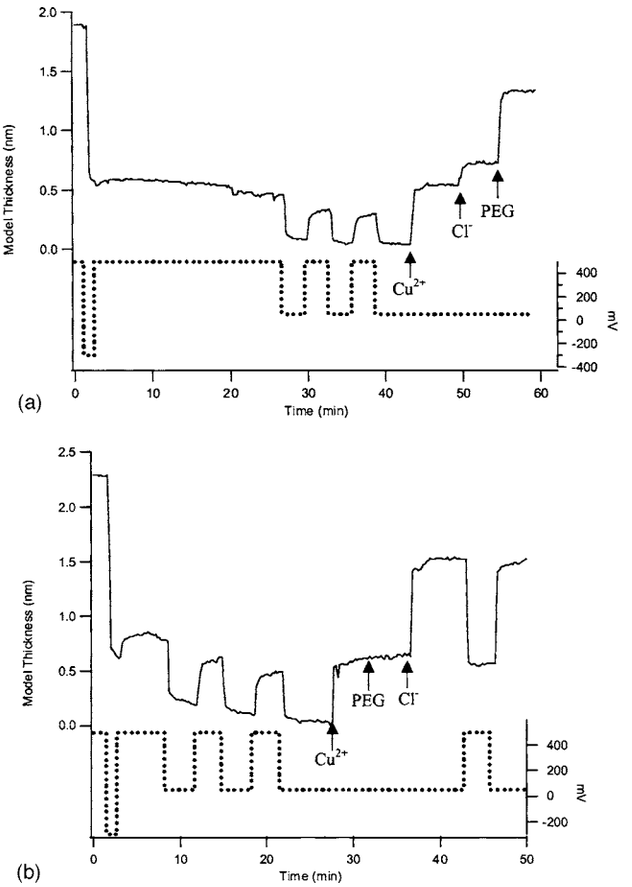

Figure 5. (a) Model thickness (solid line) of an experimental run on an activated Ru surface in which a Cu UPD layer was formed subsequent to Cu^{2+} addition (43 min), followed by the addition of Cl^- (49 min) and PEG (54 min), with all additions made at 0.050 V. (b) Model thickness (solid line) of an experimental run on an activated Ru surface in which a Cu UPD layer was formed subsequent to Cu^{2+} (27 min) addition, followed by the addition of PEG (33 min) and Cl^- (37 min), with all additions made at 0.050 V. The history of the applied potential is given by the dotted line in each case.

and 0.52 nm, see Table I) is approximately the same as that found (0.57 ± 0.05 nm) on the coinage metals positive of the pzc,[31] implying comparable hydrocarbon coverage.

Stripping and reformation of the PEG/Cl/Cu UPD/Ru overlayer formed in Fig. 5b was also examined. Specifically, at 43 min the potential was stepped to 0.50 V_{SCE}. The decrease of the model thickness to a value of 0.55 nm, near the original value at the beginning of the run at the potential of 0.50 V_{SCE}, implies desorption

Table I. Additive layer thickness in nanometers on Ru and the Cu UPD layer at 0.050 V and the monolayer oxide at 0.50 V.

Additive	Activated Ru	Cu UPD layer on Ru	Oxide monolayer on Ru
PEG	0.08 ± 0.06	0.02 ± 0.01	0.02 ± 0.01
Cl^-	0.00 ± 0.00	0.13 ± 0.10	0.01 ± 0.02
PEG + Cl^-	0.47 ± 0.02	0.78 ± 0.22	0.04 ± 0.02
Cl^- + PEG	0.43 ± 0.10	0.65 ± 0.20	0.05 ± 0.01
δPEG[a]	0.42 ± 0.09	0.52 ± 0.10	0.04 ± 0.03

[a] δPEG is defined as the difference between the model thickness for the (Cl^- + PEG) layer and the Cl^- layer alone.

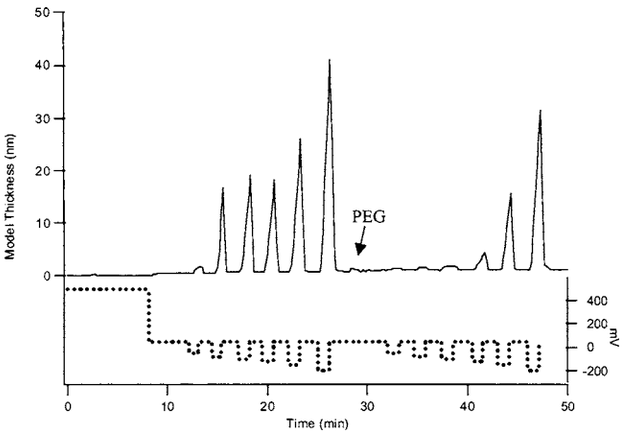

Figure 6. Model thickness (solid line) of an experimental run on an activated Ru surface in which a Cu UPD layer was formed subsequent to Cu^{2+} addition at 0.050 V. The potential (dotted line) was stepped to increasingly negative potentials for 1-min intervals, resulting in bulk metal deposition, and then stepped back to 0.050 V. PEG was added at 28 min and the potential steps repeated.

of both the Cu UPD layer and the PEG Cl^- layer. The absence of a significant PEG–Cl^- layer was confirmed by independent spectroscopic ellipsometric studies at 0.50 V_{SCE} (see Table I), indicating that the monolayer oxide formed at 0.50 V_{SCE} inhibits PEG–Cl^- adsorption. Upon subsequent potential decrease back to 0.050 V_{SCE} at 46 min, the model thickness reverted to that prior to the oxidation step at 0.50 V_{SCE}, consistent with redevelopment of the composite Cu UPD and adsorbed additive layer.

PEG–Cl^- adsorption on Ru native oxide.— Preliminary measurements on rough, ~100-nm-thick Ru films as well as more complete studies on 6.5-nm films indicate that, unlike on the activated Ru surfaces, slight nonspecific adsorption of PEG occurs on the native oxide, resulting in an ~0.2-nm model thickness film. This is comparable to the model film thickness observed for the adsorption of PEG on Au near the pzc.[31] There was no detectable increase in the model film thickness in the presence of Cl^-, indicating that the formation of a robust PEG–Cl^- layer is inhibited by the native oxide, consistent with reports of inhibition of Cl^- adsorption on oxidized Ru.[41]

PEG–Cl^- inhibition of bulk Cu deposition on Cu UPD/Ru.— Figure 6 examines the influence of PEG–Cl^- on Cu overpotential or bulk deposition (OPD). An activated Ru substrate in an electrolyte containing 1 mmol/ LCl^- was initially biased at 0.50 V_{SCE} and then stepped to 0.050 V_{SCE} to form a Cu UPD layer. The optical signal was stable, indicating a steady-state surface coverage. The potential was then stepped to a fixed value for ~1 min and then returned to 0.050 V_{SCE}. The increase in the ellipsometric model thickness corresponding to the bulk Cu deposit is evident, as is the decrease from the subsequent dissolution of the deposit. Based on the unchanged model thickness at 0.050 V_{SCE}, the Cu UPD layer remains intact after each cycle. The potential excursions were progressively increased from −(0.050 to 0.250) V_{SCE} to allow a growth velocity curve to be measured. At the conclusion of the first set of measurements, approximately 28 min into the experiment, PEG was added to the system (the increase in model thickness of ~0.5 nm associated with its adsorption is present though difficult to see for the plot dimensions used) and then the cyclic OPD experiment repeated. Significant inhibition of the plating process is evident in Fig. 6. The results are summarized as average effective deposition rate vs potential in Fig. 7. This PEG-induced inhibition is in excellent qualitative agreement with the voltammetry shown in Fig. 3, in spite of the different time scales of the potentiostatic ellipsometic experiment (minutes) and the potentiodynamic experiment (seconds based

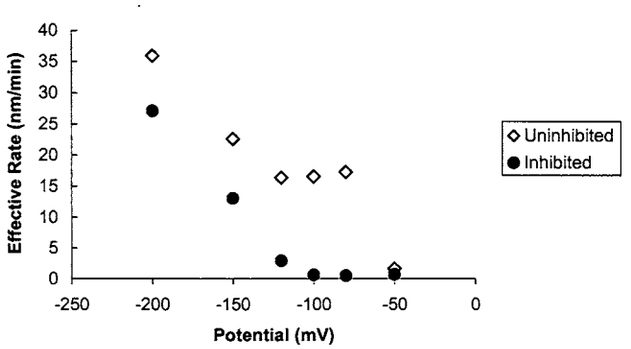

Figure 7. Effective Cu deposition rates, based on the overpotential results in Fig. 6. Uninhibited deposition in the presence of Cl^- is represented by ◇; deposition in the presence of the rate-suppressing PEG–Cl^- is represented by ●.

on 50-mV/s sweep rate). The ellipsometry experiments fully capture the PEG–Cl^- layer that is formed on the Cu UPD layer and its inhibition of bulk Cu deposition.

Discussion

Bulk electrodeposition of one metal onto a "foreign" metal substrate consists of a nucleation and growth process in which the deposited species form nuclei that grow in either a two-dimensional or three-dimensional manner. Nucleation is assumed to take place on discrete sites, the density of sites possibly being potential dependent. Conventionally, the heterogeneous nucleation and growth processes are characterized by different modes: (*i*) Volmer–Weber growth, involving the formation of nuclei on a nonwetting substrate that grow in a three-dimensional manner and eventually coalesce, typically forming rough films; (*ii*) Frank van der Merwe or layer-by-layer growth, which normally results in smooth films; (*iii*) Stranski–Krastanov growth, where a three-dimensional growth occurs on a two-dimensional wetting layer, which can also result in smooth films.[43] Control of surface chemistry to promote a surface that Cu easily wets and successfully plates is one of the key challenges to the use of Ru as a barrier or liner material for Cu metallization. In this study we have investigated the adsorption of PEG and Cl^-, two important additive components of superfilling electroplating baths, on Ru in order to address one aspect of this complex problem. The interaction between Cu UPD and adsorbed additives received close attention as it directly impacts the nucleation and growth of Cu on Ru. Furthermore, from a surface analytical perspective, the interaction between Cu UPD and plating additives can be studied free of the measurement challenges associated with studying a moving interface such as exists during bulk copper deposition or dissolution.

The adsorption and impact of PEG and Cl^- on Cu surfaces has been widely studied.[24-32] The inhibiting effect toward Cu electrodeposition of these two additives in competition with the accelerating effect of SPS is essential to successful superfill of patterned features. On Ru, the surface chemistry must be tailored to promote controlled direct electrodeposition. Most significantly, in other work[16] it has been demonstrated that smooth Cu films can be obtained by plating on activated Ru surfaces in the presence of PEG–Cl^-, whereas plating on the oxidized, nonwetting substrates proceeds by a Volmer–Weber growth mode and yields films that are rough and poorly adherent to the substrate.

In this study we have demonstrated that a PEG–Cl^- layer forms on both activated Ru substrates and the Cu UPD layer, implying that the chemistry that underlies superfill via the curvature-enhanced accelerator coverage model[2,16] is not significantly perturbed. This is further supported by the observation that the PEG–Cl^- layer coadsorbed on the Cu UPD layer inhibits Cu bulk electrodeposition as compared to deposition in the absence of the additives in the electrolyte. These observations are consistent with good bottom-up filling on Ru surfaces that are devoid of the native oxide.[16] In contrast, we have observed that both monolayer oxides and the native oxide inhibit the development of a significant PEG–Cl^- layer. This is consistent with the absence of inhibition of Cu electrodeposition initially observed on the native oxide prior to Cu cluster coalescence.[16] As the PEG–Cl layer is essential to effective bottom-up feature filling, these results suggest that a Cu UPD layer can be engineered as a platform for optimizing the growth process and represents a promising avenue for further research and optimization of Cu damascene processing.

The National Institute of Standards and Technology assisted in meeting the publication costs of this article.

References

1. P. C. Andricacos, C. Uzoh, J. O. Dukovic, J. Horkans, and H. Deligianni, *IBM J. Res. Dev.*, **42**, 567 (1998).
2. T. P. Moffat, D. Wheeler, M. D. Edelstein, and D. Josell, *IBM J. Res. Dev.*, **49**, 19 (2005).
3. A. E. Kaloyeros, X. M. Chen, T. Stark, K. Kumar, S. Seo, G. G. Peterson, H. L. Frisch, B. Arkles, and J. Sullivan, *J. Electrochem. Soc.*, **146**, 170 (1999).
4. A. Radisic, J. G. Long, P. M. Hoffmann, and P. C. Searson, *J. Electrochem. Soc.*, **148**, C41 (2001).
5. A. Radisic, Y. Cao, P. Taephaisitphongse, A. C. West, and P. C. Searson, *J. Electrochem. Soc.*, **150**, C362 (2003).
6. L. Magagnin, A. Vicenzo, M. Bain, H. W. Toh, H. S. Gamble, and P. L. Cavallotti, *Microelectron. Eng.*, **76**, 131 (2004).
7. S. K. Kim, S. K. Cho, J. J. Kim, and Y. S. Lee, *Electrochem. Solid-State Lett.*, **8**, C19 (2005).
8. Y. Cao, J. M. Lee, and A. C. West, *Plat. Surf. Finish.*, **90**, 40 (2003).
9. H. Deligianni, J. O. Dukovic, E. G. Walton, R. J. Contolini, J. Reid, and E. Patton, in *Electrochemical Processing in ULSI Fabrication and Semiconductor/Metal Depostion II*, P. C. Andricacos, P. C. Searson, C. Reidsema-Simpson, P. Allongue, J. L. Stickney and G. M. Oleszek, Editors, PV 99-9, p. 83, The Electrochemical Society Proceedings Series, Pennington, NJ (1999).
10. M. Matlosz, P. H. Vallotton, A. C. West, and D. Landolt, *J. Electrochem. Soc.*, **139**, 752 (1992).
11. O. Chyan, T. N. Arunagiri, and T. Ponnuswamy, *J. Electrochem. Soc.*, **150**, C347 (2003).
12. D. Josell, D. Wheeler, C. Witt, and T. P. Moffat, *Electrochem. Solid-State Lett.*, **6**, C143 (2003).
13. M. W. Lane, C. E. Murray, F. R. McFeely, P. M. Vereecken, and R. Rosenberg, *Appl. Phys. Lett.*, **83**, 2330 (2003).
14. R. Chan, T. N. Arunagiri, Y. Zhang, O. Chyan, R. M. Wallace, M. J. Kim, and T. Q. Hurd, *Electrochem. Solid-State Lett.*, **7**, G154 (2004).
15. T. N. Arunagiri, Y. Zhang, O. Chyan, M. El Bouanani, M. J. Kim, K. H. Chen, C. T. Wu, and L. C. Chen, *Appl. Phys. Lett.*, **86**, 083104 (2005).
16. T. P. Moffat, P. J. Chen, M. L. Walker, J. E. Bonevich, W. F. Egelhoff, D. Wheeler, L. J. Richter, and D. Josell, *J. Electrochem. Soc.*, **153**, C37 (2006).
17. A. Aramata, in *Modern Aspects of Electrochemistry*, J. O. Bockris, R. E. White, and B. E. Conway, Editors, p. 181, Plenum Press, New York (1997).
18. E. Herrero, L. J. Buller, and H. D. Abruna, *Chem. Rev. (Washington, D.C.)*, **101**, 1897 (2001).
19. D. M. Kolb, in *Advances in Electrochemistry and Electrochemical Engineering*, H. Gerischer and C. Tobias, Editors, p. 125, John Wiley & Sons, New York (1978).
20. E. M. Stuve, J. W. Rogers, D. Ingersoll, D. W. Goodman, M. L. Thomas, and M. T. Paffett, *Chem. Phys. Lett.*, **149**, 557 (1988).
21. C. N. Van Huong and M. J. Gonzalez-Tejera, *J. Electroanal. Chem. Interfacial Electrochem.*, **244**, 249 (1988).
22. K. R. Zavadil, D. Ingersoll, and J. W. Rogers, *J. Electroanal. Chem. Interfacial Electrochem.*, **318**, 223 (1991).
23. Y. B. Zhang, L. Huang, T. N. Arunagiri, O. Ojeda, S. Flores, O. Chyan, and R. M. Wallace, *Electrochem. Solid-State Lett.*, **7**, C107 (2004).
24. Z. V. Feng, X. Li, and A. A. Gewirth, *J. Phys. Chem. B*, **107**, 9415 (2003).
25. M. Hayase, M. Taketani, K. Aizawa, T. Hatsuzawa, and K. Hayabusa, *Electrochem. Solid-State Lett.*, **5**, C98 (2002).
26. J. P. Healy, D. Pletcher, and M. Goodenough, *J. Electroanal. Chem.*, **338**, 155 (1992).
27. M. R. H. Hill and G. T. Rogers, *J. Electroanal. Chem. Interfacial Electrochem.*, **86**, 179 (1978).
28. J. J. Kelly and A. C. West, *J. Electrochem. Soc.*, **145**, 3472 (1998).
29. T. P. Moffat, D. Wheeler, and D. Josell, *J. Electrochem. Soc.*, **151**, C262 (2004).
30. M. Petri, D. M. Kolb, U. Memmert, and H. Meyer, *J. Electrochem. Soc.*, **151**, C793 (2004).
31. M. L. Walker, L. J. Richter, and T. P. Moffat, *J. Electrochem. Soc.*, **152**, C403 (2005).
32. M. L. Walker, L. J. Richter, and T. P. Moffat, Unpublished data.
33. F. Chao, M. Costa, and A. Tadjeddine, *J. Electroanal. Chem.*, **329**, 313 (1992).
34. S. Gottesfeld, Y. T. Kim, and A. Redondo, in *Physical Electrochemistry*, I. Rubinstein, Editor, p. 393, Marcel Dekker, New York (1995).
35. D. M. Kolb, in *Spectroelectrochemistry*, R. J. Gale, Editor, p. 87, Plenum Press, New York (1988).
36. N. S. Marinkovic, J. X. Wang, H. Zajonz, and R. R. Adzic, *J. Electroanal. Chem.*,

500, 388 (2001).
37. J. X. Wang, N. S. Marinkovic, H. Zajonz, B. M. Ocko, and R. R. Adzic, *J. Phys. Chem. B*, **105**, 2809 (2001).
38. S. Hadzijordanov, H. Angersteinkozlowska, M. Vukovic, and B. E. Conway, *J. Electrochem. Soc.*, **125**, 1471 (1978).
39. R. O. Lezna, N. R. Detacconi, and A. J. Arvia, *J. Electroanal. Chem. Interfacial Electrochem.*, **151**, 193 (1983).
40. D. Michell, D. A. J. Rand, and R. Woods, *J. Electroanal. Chem. Interfacial Electrochem.*, **89**, 11 (1978).
41. G. Horanyi and E. M. Rizmayer, *J. Electroanal. Chem. Interfacial Electrochem.*, **181**, 199 (1984).
42. K. Doblhofer, S. Wasle, D. M. Soares, K. G. Weil, G. Weinberg, and G. Ertl, *Z. Phys. Chem. (Munich)*, **217**, 479 (2003).
43. M. A. Schneeweiss and D. M. Kolb, *Phys. Status Solidi A*, **173**, 51 (1999).